Modularity of a carbon-fixing protein organelle

Walter Bonacci[a], Poh K. Teng[b], Bruno Afonso[a], Henrike Niederholtmeyer[a], Patricia Grob[c], Pamela A. Silver[a,d], and David F. Savage[b,e,1]

[a]Department of Systems Biology, Harvard Medical School, Boston, MA 02115; [b]Department of Molecular and Cell Biology and [c]Howard Hughes Medical Institute, University of California, Berkeley, CA 94720; [d]Wyss Institute for Biologically Inspired Engineering, Harvard University, Boston, MA 02115; and [e]Department of Chemistry, University of California, Berkeley, CA 94720

Edited* by Robert M. Stroud, University of California, San Francisco, CA, and approved November 17, 2011 (received for review May 31, 2011)

Bacterial microcompartments are proteinaceous complexes that catalyze metabolic pathways in a manner reminiscent of organelles. Although microcompartment structure is well understood, much less is known about their assembly and function in vivo. We show here that carboxysomes, CO_2-fixing microcompartments encoded by 10 genes, can be heterologously produced in *Escherichia coli*. Expression of carboxysomes in *E. coli* resulted in the production of icosahedral complexes similar to those from the native host. In vivo, the complexes were capable of both assembling with carboxysomal proteins and fixing CO_2. Characterization of purified synthetic carboxysomes indicated that they were well formed in structure, contained the expected molecular components, and were capable of fixing CO_2 in vitro. In addition, we verify association of the postulated pore-forming protein CsoS1D with the carboxysome and show how it may modulate function. We have developed a genetic system capable of producing modular carbon-fixing microcompartments in a heterologous host. In doing so, we lay the groundwork for understanding these elaborate protein complexes and for the synthetic biological engineering of self-assembling molecular structures.

ribulose 1,5-bisphosphate carboxylase/oxygenase | synthetic biology | metabolic engineering | self-assembly

The spatial organization of incompatible processes is a fundamental design principle of biological systems (1). For example, metabolic pathways are confined to specific organelles as a means of ensuring pathway fidelity, catalyzing reactions against the chemical equilibrium of other compartments, and limiting exposure to toxic intermediates (2). Despite the generality of this strategy in nature, the ability to rationally organize processes in vivo remains a major challenge to bioengineering (3). Recent work has demonstrated that engineering protein–protein interactions using molecular scaffolds can be used to rewire signaling networks and improve metabolic pathways (4, 5). A desirable extension of this modularity would be the ability to rationally organize pathways or networks in a topologically distinct compartment, or synthetic organelle. If available, a synthetic organelle would have numerous applications in bioengineering, nanotechnology, and particularly metabolic engineering, where it could be used to improve the rate and yield of cellular chemical reactions while lowering toxicity to the host.

One biological assembly that could form the basis of such a synthetic organelle is the bacterial microcompartment (BMC). BMCs are enzyme-containing proteinaceous complexes that catalyze metabolic pathways incongruous with the cytoplasm (Fig. 1). Structurally, BMCs are formed from thousands of shell proteins that self-assemble into an icosahedral structure 100–200 nm in diameter (Fig. 1*A*) (6–8). These shell proteins surround a lumen containing tens to hundreds of copies of two to four specific enzymes that constitute a short metabolic pathway. This metabolic pathway is the distinguishing feature between BMC compartments of different organisms. There are currently three known classes of BMCs: the CO_2-fixing carboxysome (CB), the 1,2-propanediol utilization microcompartment (PDU), and the ethanolamine utilization microcompartment (9). BMC protein domains appear in roughly 20% of bacteria, suggesting the existence of a large functional diversity of uncharacterized BMCs (10).

The CB was the first BMC to be discovered and remains a model system for elucidating how BMCs assemble and function in the cell (11). Its shell is assembled from roughly 800 protein hexamers, which form the facets of the icosahedron, and 12 pentamers, which form the vertices (8, 12). Inside the lumen are the enzymes ribulose 1,5-bisphosphate carboxylase/oxygenase (RuBisCO) and carbonic anhydrase (CA), which are directed to this location by protein–protein interactions with the shell and/or shell interaction mediators (13). Depending on the organism, genes for these shell proteins and luminal enzymes can occur either together in a single operon or, alternatively, in several operons across the genome (9).

Biochemically, the CB plays a central role in the carbon-concentrating mechanism (CCM) (14, 15). In the CCM, inorganic carbon (i.e., CO_2 and bicarbonate) is actively transported into the cell. Bicarbonate, the major inorganic carbon species at pH ~7, passively diffuses across the CB shell and is rapidly converted by CA into CO_2. Alone, RuBisCO exhibits both low CO_2 affinity and low selectivity against the competing substrate O_2. In the context of the CCM, however, it is postulated that the CB lumen contains elevated levels of CO_2 and that RuBisCO is able to fix CO_2 near its V_{max} with high specificity. After fixation, the product 3-phosphoglycerate diffuses out of the carboxysome and enters the central carbon metabolism (Fig. 1*B*). High local concentrations of CO_2 and the possible selective nature of the shell proteins may be instrumental in excluding the competing RuBisCO substrate O_2 from the lumen, but this hypothesis remains unproven. In other BMCs, the shell is known to act as a barrier to prevent both the loss and toxicity of pathway intermediates (16, 17). Finally, it was recently shown that a unique class of trimeric shell proteins with pseudo-sixfold symmetry, notably CsoS1D, forms larger pores and shows evidence of gating, suggesting that these proteins may be crucial to substrate and product permeability (18, 19).

Recent work has focused on the modularity of BMC assembly. In the case of the CB from *Halothiobacillus neapolitanus,* in which all genes occur in a single operon, deletion of RuBisCO-encoding genes was found to lead to empty, yet morphologically well-formed shells (20). This finding suggests that BMCs form robust structures in which alternative proteins could be loaded inside the lumen. We recently reported that proteins can be targeted to the CB via fusion with CB proteins such as RuBisCO (21). Work on the PDU has confirmed this modularity. A genetic screen in *Citrobacter freundii* led to the isolation and refinement of a single PDU regulon sequence for expressing functional

Author contributions: W.B., P.K.T., B.A., P.A.S., and D.F.S. designed research; W.B., P.K.T., H.N., P.G., and D.F.S. performed research; P.G. contributed new reagents/analytic tools; W.B., P.K.T., P.A.S., and D.F.S. analyzed data; and W.B., P.A.S., and D.F.S. wrote the paper.

The authors declare no conflict of interest.

*This Direct Submission article had a prearranged editor.

[1]To whom correspondence should be addressed. E-mail: dsavage@berkeley.edu.

This article contains supporting information online at www.pnas.org/lookup/suppl/doi:10.1073/pnas.1108557109/-/DCSupplemental.

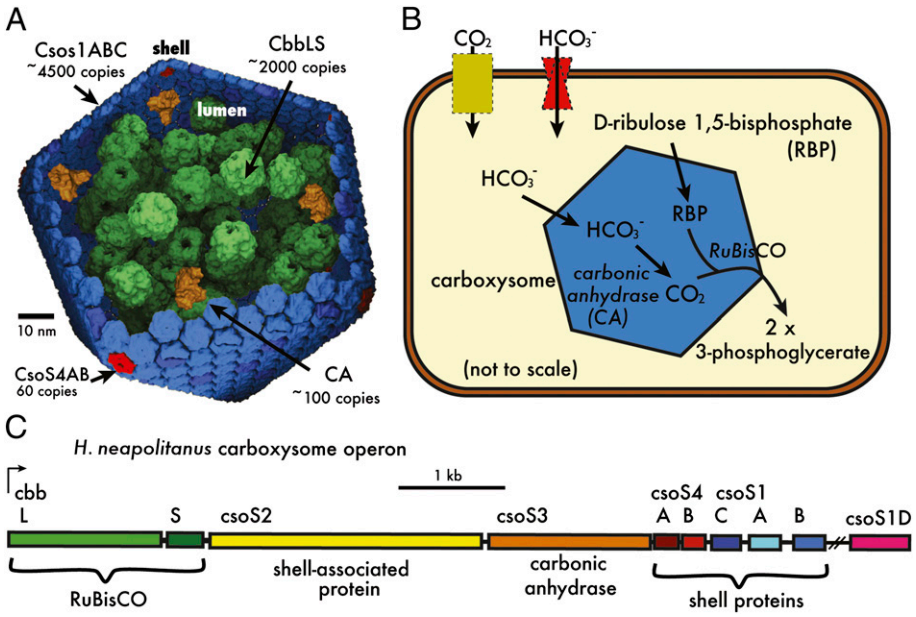

Fig. 1. Physical and genetic organization of the carboxysome. (*A*) Molecular surface representation of a partial model of the carboxysome showing RuBisCO (green), carbon anhydrase (orange), CsoS1ABC (blue), and CsoS4AB (red). (*B*) Schematic of the carbon concentrating mechanism adapted from Kaplan and Reinhold (14). (*C*) Genomic organization of the carboxysome operon in *H. neapolitanus*. Colors match the structural model in *A*.

compartments in *Escherichia coli* (22, 23). In addition, a putative N-terminal signal sequence capable of loading new proteins into the PDU has been isolated; however, a targeting sequence has not yet been elucidated for CB proteins (20, 24). Thus, although the present work indicates that BMCs are capable of acting as modular protein assemblies, more characterization is needed before BMCs are ready for use in bioengineered systems.

Ultimately, a synthetic organelle will require both simplicity, to facilitate the engineering process, and extensibility, to enable a variety of functions. In the context of the BMC, these characteristics set molecular constraints, which must be clarified through genetic and protein engineering. These constraints include a description of the genes necessary and sufficient for functional expression in an arbitrary host, an understanding of shell selectivity to allow tuning of permeability to the desired function, and a clear targeting mechanism for specifying cargo. First and foremost, however, is the development of a model BMC to facilitate rapid optimization of the molecular chassis.

Toward this end, here we present a genetic system for the heterologous expression of functional BMCs. We show that expression of the CB regulon from *H. neapolitanus* results in the formation of functional CBs in *E. coli*. We also show that the purified synthetic CBs contain the proper protein constituents and exhibit CO_2 fixation activity. Overall, our findings demonstrate the ability to heterologously produce modular and functional carbon-fixing BMCs. By doing so, we lay the groundwork for the future design of protein-based synthetic organelles, including the engineering of compartmentalized biological processes.

Results

Heterologous Formation of Carboxysomes. CBs are classified as either α-type or β-type based on their RuBisCO coding sequence. Generally, α-CBs also display a simplified regulatory structure in which all genes are found together at a single genomic locus (25, 26). Thus, we reasoned that using an α-type CB operon could simplify the expression of functional particles in a heterologous host. We cloned the α-type CB operon from *H. neapolitanus* (HnCB) containing nine genes into the isopropyl β-D-1-thio-galactopyranoside (IPTG)-inducible plasmid pNS3 (pHnCB) and investigated expression of the HnCB in *E. coli*.

We observed the formation of CBs in *E. coli* expressing the *H. neapolitanus* operon. Cells containing pHnCB were induced with IPTG and analyzed using ultrathin sectioning and electron microscopy (EM). As expected, the presence and morphology of CBs was highly dependent on IPTG concentration. In the absence of IPTG, cells generally had between zero and two icosahedral structures per cell (Fig. 2*A*). This was presumably from leaky expression of the pNS3 promoter, given that WT *E. coli*

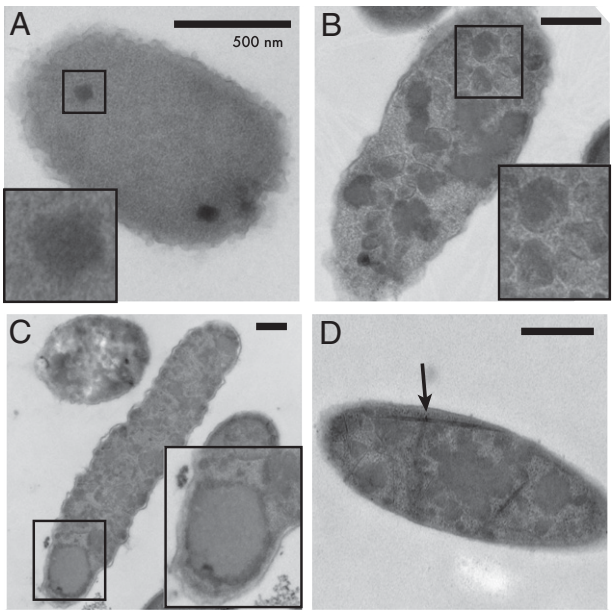

Fig. 2. Electron microscopy of carboxysomes in vivo. (*A*) Expression of HnCB at 0 μM IPTG. (*B*) Same as *A* but at 50 μM IPTG. (*Inset*) Icosahedral structures. (*C*) Same as *A*, but at 200 μM IPTG. (*Inset*) Inclusion body. (*D*) Appearance of filaments (arrow) under high induction conditions. (Scale bars: 500 nm.)

contained no such structures (Fig. S1). These structures resembled CBs from *H. neapolitanus* (12). At higher induction (50 and 200 μM IPTG), the cells contained an increasing number of CBs such that the entire cytoplasm was eventually filled and the cells became filamentous (Fig. 2 *B* and *C*). Many CBs were of varying contrast with dense shell edges and lighter facets, reminiscent of CBs containing a partial load of enzyme cargo (20). Higher induction also led to a number of defects, including inclusion body formation and the appearance of linear filaments, possibly indicating an imbalance in protein stoichiometry (Fig. 2*C*, *Inset* and *D*). High-resolution images are shown in Fig. S1.

Assembly and Function of Carboxysomes. One assay to evaluate microcompartment assembly involves the ability to target fluorescently tagged proteins to nascent particles. We recently showed that various full-length CB proteins fused to GFP can be targeted to functional CBs in the cyanobacterium *S. elongatus* PCC7942 (21).

As in the native host, synthetic CBs in *E. coli* were assembled with labeled cargo and could be imaged using fluorescence microscopy. CsoS1A, a major shell protein, and CbbL, the large subunit of RuBisCO, were fused with a C-terminal GFP and CFP, respectively, and cloned into the IPTG-inducible, kanamycin-resistant vector pDFS21, which is suitable for cotransformation with the pNS3 plasmid. Control expression of GFP or CFP alone or with HnCB yielded no foci, consistent with unaggregated cytoplasmic fluorescent protein (Fig. S2).

Expression of CsoS1A-GFP in the absence of HnCB gave rise to large polar foci (Fig. 3*A*) that appear similar to inclusion bodies, and is nearly identical to expression of PDU subunits PduD and PduV in the absence of shell proteins (23). Given CsoS1A's hexameric quaternary structure and role as a major component of the CB shell in vivo (Fig. 1*A*), that this overexpression could result in the runaway formation of protein aggregates is not surprising (27). Expression of the remaining BMC operon did not appear to decrease inclusion body formation, but did result in the faint appearance of cytoplasmic foci (Fig. 3*B*, white arrow), consistent with labeled BMCs. In the previous PDU study, neither protein component was found to be a major shell protein; thus, CsoS1A's continued aggregation in the presence of the remaining HnCB proteins could be a result of its inherent propensity toward self-assembly.

Like CsoS1A-GFP, expression of CbbL-CFP gave rise to polar assemblies (Fig. 3*C*). CbbL normally associates with the small subunit CbbS in forming holo-RuBisCO. Expression of CbbL in the absence of CbbS or even the remaining CB proteins could lead to the formation of inclusion bodies. The large subunit's inherent propensity toward self-assembly is well known (28), and the accumulations observed in the present study support the hypothesis that RuBisCO plays a role in BMC assembly (13, 20). However, on coexpression of HnCB, we observed a decrease in inclusion body signal and the formation of distinct foci throughout the *E. coli* cytoplasm (Fig. 3*D*). These foci are reminiscent of labeled CBs in *Synechococcus elongatus* and are consistent with CFP-labeled CbbL being targeted to assembling and mature CB structures (21).

Given that the CBs appear to assemble correctly, we asked whether the complexes are functional in vivo. In the native host, CBs carry out the defining step of the Calvin–Benson–Basham cycle, the fixation of CO_2 and D-ribulose 1,5-bisphosphate, to produce two molecules of 3-phosphoglycerate. A heterotrophic host catabolizing sugar is incapable of carrying out a complete CO_2 fixation cycle; however, a physiological strategy for testing CO_2 fixation has been developed recently (29). As part of pentose phosphate metabolism, *E. coli* normally converts arabinose to D-ribulose 5-phosphate (Fig. 3*E*). Expression of phosphoribulokinase (PRK) results in the irreversible buildup of D-ribulose 1,5-bisphosphate and a concomitant growth defect as a result of diverted carbon flux away from biosynthetic intermediates; however, coexpression of RuBisCO, leads to the rescue of growth via the conversion of accumulated D-ribulose 1,5-bisphosphate into 3-phosphoglycerate.

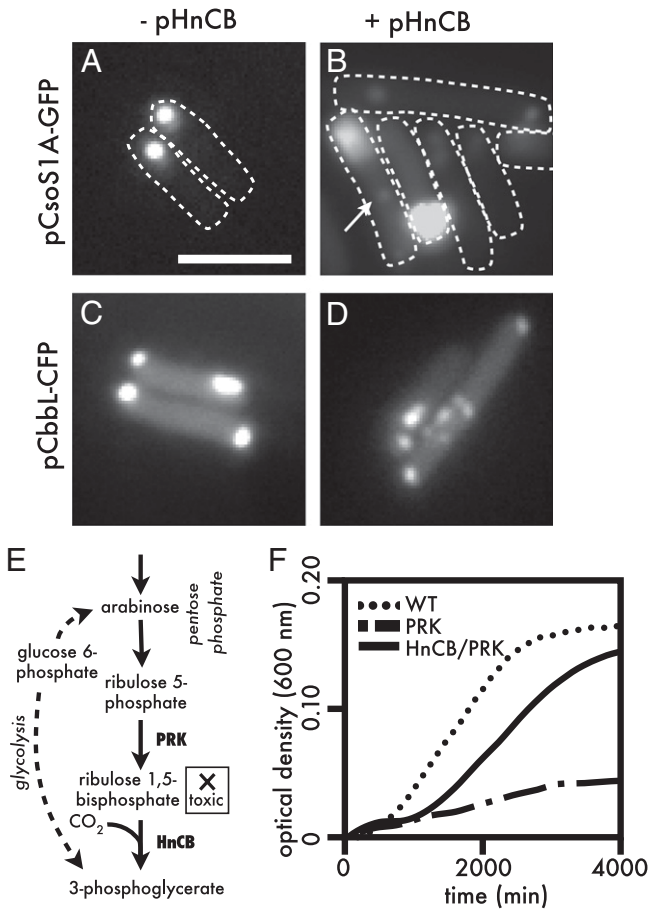

Fig. 3. Carboxysomes assemble and are functional in vivo. (*A–D*) Microscopy images of cells expressing fluorescently labeled carboxysome components in the presence and absence of pHnCB. (Scale bar: 2.5 μm.) Controls are shown in Fig. S2. The arrow in *B* highlights a likely CB particle. (*E*) Schematic of metabolic complementation strategy. (*F*) Representative growth curves of WT, pPRK, and pPRK/pHnCB strains showing complementation via carbon fixation.

We used the growth regimen described earlier to demonstrate HnCB-dependent CO_2 fixation. The gene encoding PRK was cloned from *S. elongatus* PCC7942 into pDFS21 (pPRK) to allow simultaneous coexpression with pHnCB. In the presence of both arabinose and bicarbonate, expression of PRK in log-phase cells resulted in increased doubling time (16.3 ± 9.0 h; $n = 3$ for all) compared with WT cells (5.4 ± 1.6 h), consistent with the D-ribulose 1,5-bisphosphate toxicity reported previously (29). Coexpression with HnCB resulted in rescue of growth. Cultures had exponential growth rates (6.9 ± 2.5 h) similar to that of WT but displayed a slightly longer initial lag phase, presumably due to the increased burden of producing both PRK and HnCB proteins. A representative growth curve is shown in Fig. 3*F*. This suggests that expression of HnCB can be used to create functional BMCs capable of fixing CO_2 in the normally heterotrophic host *E. coli*.

Characterization of Purified Carboxysomes. To further demonstrate the functionality of heterologous CBs, we purified particles using sucrose gradient centrifugation and characterized them in vitro. Negative-stain EM revealed that purified CBs were somewhat icosahedral in shape (albeit less so than purified particles from the native host) and contained a large number of torus-shaped

RuBisCO octomers (Fig. 4*A*). The average size of the purified CBs was 136 ± 30 nm (n = 34), a slightly larger size than *H. neapolitanus*-derived CBs (7). Like some in vivo particles described earlier (Fig. 2*D*), many CBs displayed either unfilled lumen spaces or defective shells, possibly the result of partial assembly or disrupted morphology (Fig. 4*A*). RuBisCO octomers also were occasionally visible outside of CBs (Fig. 4*A*, box).

A tenth gene, *csoS1D*, located in the genome just outside of the core operon, was recently discovered (18). Its gene product is thought to play a role in shell permeability, and so we next investigated how the addition of this protein could affect CB structure and function (19). *csoS1D* was cloned into pHnCB downstream of the operon to create the plasmid pHnCBS1D and then expressed in *E. coli*. Imaging of purified particles by negative-stain EM showed them to be slightly smaller than those expressed from pHnCB (117 ± 25 nm; n = 30). Interestingly, the morphology was more reminiscent of CBs from *H. neapolitanus* than of CBs from *E. coli* cells expressing pHnCB (Fig. 4*B*). The addition of CsoS1D may be important for CB assembly, given that only 35% (n = 23) of these structures displayed shell defects, compared with 68% (n = 22) of those for the nine-gene construct.

The protein constituents of purified CBs were verified via gel electrophoresis followed by liquid chromatography–mass spectrometry. CBs isolated from cells expressing pHnCBS1D were analyzed by SDS/PAGE, and prominent bands were extracted, trypsinized, and analyzed by mass spectrometry (Fig. 4*C*). Using this strategy, we detected CsoS2AB, CbbL, CbbS, and CsoS1ABC, but did not observe a significant band for CsoS3. Interestingly, we were able to detect CsoS1D as a faint band running near its theoretical MW of 23.5 kDa, which has not been reported previously (12). Quantitation of the relative amount of signal for each of these components (Fig. S3*A*) was similar to that reported by Cannon and Shively (30), except for a slight increase in CbbL content and a decrease in CbbS content.

We used a simple centrifugation assay to investigate the integrity of heterologous CBs and examine whether RuBisCO is associated with CBs or free in solution. CBs are known to sediment at relatively low force (e.g., 14,000 × g), so we centrifuged purified CBs to assess RuBisCO location (31). Supernatant and pelleted fractions were analyzed by SDS/PAGE, and Coomassie blue-stained bands were quantified, revealing that 77% of RuBisCO was associated with carboxysomes (Fig. S3*B*).

Finally, we verified the in vitro activity of purified CBs. Carbon fixation was measured by recording 3-phosphoglycerate–dependent NADH oxidation in a coupled enzyme reaction system. Initial enzymatic rates were measured under varying concentrations of the substrate D-ribulose 1,5-bisphosphate (Fig. 4*D*), and the data were fit to a Michaelis–Menten model using nonlinear regression. The affinity for D-ribulose 1,5-bisphosphate between CB preparations was similar, with determined K_m values of 200 ± 30 μM for pHnCB and 204 ± 71 μM for pHnCBS1D. Activity was higher in the pHnCB-derived CBs, however (V_{max} value, 11.7 ± 0.5 μmol·min^{-1}·mg^{-1}, compared with 6.9 ± 0.3 μmol·min^{-1}·mg^{-1} for pHnCBS1D). The K_m value is similar to that previously reported for purified CBs from *H. neapolitanus* (174 μM), whereas the rate is higher (1.7 μmol·min^{-1}·mg^{-1}) (32).

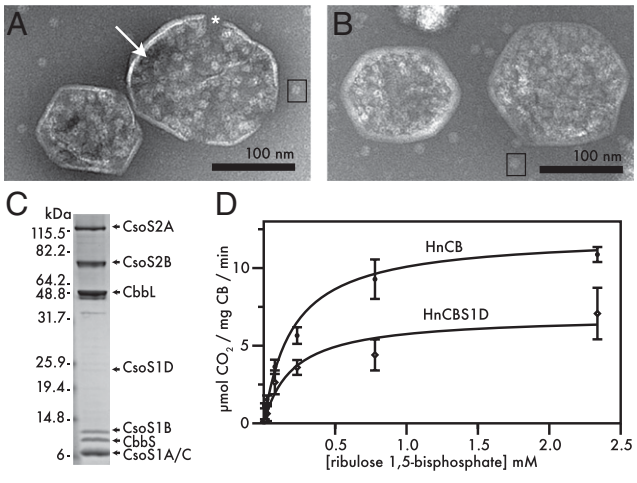

Fig. 4. Characterization of purified carboxysomes. (*A*) Representative electron microscopy image of purified carboxysomes expressed using the pHnCB plasmid. The arrow indicates a low-density lumen area, the asterisk indicates a shell defect, and the box highlights the RuBisCO octomer. (Scale bar: 100 nm.) (*B*) Same as *A*, but of purified carboxysomes expressed using the pHnCBS1D plasmid. (*C*) SDS/PAGE gel of purified carboxysomes from *B* with annotated proteomics data (arrows). (*D*) Carbon fixation activity of preparations imaged in *A* and *B* as a function of D-ribulose 1,5-bisphosphate concentration. Error bars represent SD.

Discussion

Modular Expression of CBs in Nonnative Hosts. It has been postulated that α-type CBs are synthesized from a single operon containing all of the necessary genetic components for mature particle formation (33). Here we validate this hypothesis by demonstrating that heterologous expression of the CB genomic locus from *H. neapolitanus*, containing 10 genes encoding enzymes and shell proteins, is sufficient to synthesize BMCs in *E. coli* that are very similar to those of the native host. EM imaging of particles both in situ and in vitro shows that heterologous HnCB complexes display the same icosahedral morphology as CBs from *H. neapolitanus*. GFP-based fluorescence microscopy indicates that cargo proteins are targeted to assembling CBs. Moreover, HnCBs are capable of fixing CO_2 both within *E. coli* and in isolation. Thus, we have determined the genetic information sufficient for transplanting a carbon-fixing protein organelle into new hosts that otherwise do not reductively fix carbon.

One potential area for improving the function of the synthetic CBs is optimization of the HnCB operon for specific hosts. Our microscopy and biochemical data suggest both a propensity toward inclusion body formation and malformation of some CB structures (Fig. 4 *A* and *B*). Most likely, the regulation of expression for each HnCB protein is partially lost in the translation from *H. neapolitanus* to *E. coli*. In *H. neapolitanus*, expression from the HnCB operon results in a 10-fold steady-state mRNA copy number variation for the individual genes, presumably by regulation from *cis* sites and mRNA structure (33). Translation of this varied pool of mRNA, which is regulated by numerous factors including RNA secondary structure, ribosomal binding site strength, and codon use, ultimately results in a copy number difference of two orders of magnitude between the most and least expressed proteins (Fig. 1*A*). Misinterpretation of this regulation in *E. coli* could lead to the synthesis of a slightly incorrect stoichiometry for each type of HnCB protein, such that particles are generally well formed but display elements of malformation.

A second area of investigation is shell structure and permeability. Heterologous CBs containing the shell protein CsoS1D are reminiscent of CBs from *H. neapolitanus* despite the fact that CsoS1D is a minor component (Fig. 4*C*), suggesting an essential role for this protein in assembly. CsoS1D also might play a role in activity, given the lower V_{max} values in CBs containing CsoS1D than in CBs without this protein. Accordingly, it is tempting to posit a specific role of CsoS1D in modulating activity, but, unfortunately, we cannot distinguish between this possibility and the general effect of morphologically disrupted structures seen in the pHnCB construct (Fig. 4*A*). Thus, systematically exploring the expression level of each protein, especially CsoS1D, will be essential in elucidating the structural and functional for each component.

Synthetic Bacterial Microcompartments for Biotechnology and Nanotechnology. Photosynthetic CO_2 fixation dominates anthropogenic carbon emissions (roughly 120 Pg yr^{-1} vs. 7 Pg yr^{-1}), and biologically catalyzed carbon fixation is clearly essential to both fulfilling society's demand for liquid transportation fuels and mitigating the effects of greenhouse gases (34). The central enzymatic player in these carbon-fixation reactions, RuBisCO, is both slow and nonselective, and most oxygenic photosynthesizers have evolved elaborate mechanisms for dealing with these deficiencies (35). One current model for the CB is that it facilitates the fixation process by increasing the local concentration of CO_2 near RuBisCO, thereby allowing the enzyme to function closer to its V_{max} with high specificity. By taking advantage of the modularity and portability demonstrated here, CBs could be used to engineer unique carbon-fixing organisms or improve the fitness of existing oxygenic photosynthesizers. For instance, there is an emerging interest in developing bacteria capable of taking up electrons and using this reducing power to fix carbon as a means of synthesizing energy-dense molecules from electricity (36). Alternatively, it has been postulated that C3 plant production could be improved through the introduction of an improved carbon-concentrating mechanism. In such a scheme, integration of the CB and its associated transporters could result in lower water and nitrogen use, while simultaneously improving overall yields (15).

Due to their inherent modularity, CBs are also an attractive molecular chassis for engineering cellular functions beyond carbon fixation. Recent work has shown that BMCs facilitate substrate channeling while minimizing the loss of intermediates between consecutive enzymatic steps and thus improve metabolic processes in much the same way as organelles. Although the spatial engineering of enzymes on protein scaffolds can be used to improve the flux of molecules through metabolic pathways, there is currently no way to compartmentalize reactions in vivo in a similar manner (5). Fundamentally, BMCs are molecular compartments that could serve this function.

In addition, BMCs also may find uses beyond biology as nanometer-scale configurable molecular devices. A major goal of nanotechnology is to develop molecular systems that are homogenous, modular, robust, have favorable self-assembly properties, and are easy to chemically functionalize. Viral capsids display many of these properties, and a number of self-assembling viral proteins have been engineered for the construction of nanocrystals with novel optoelectrical properties (37, 38). Much of this work has centered around the use of chemically modified viral capsid proteins to create particles that are loaded with cargo and assembled ex vivo (39). BMCs offer the same supramolecular advantages, yet assemble in vivo under moderate conditions via a modular protein-based cargo targeting system, and thus may be a more general system. However, engineering BMCs will require (*i*) identification of the genes necessary and sufficient for robust shell formation, (*ii*) improved understanding of shell permeability and how its selectivity might be altered, and (*iii*) development of a targeting system such that novel cargo proteins can be selectively integrated into assembling structures. To this end, we have elucidated here a modular genetic system for expressing functional carbon-fixing BMCs that lays the groundwork for the future engineering of synthetic microcompartments.

Materials and Methods

Cloning and Cell Culture. Genes (Table S1) were cloned from purchased genomic DNA (strain ATCC 23641) into either pNS3 or pDFS21 using the oligos listed in Table S2 (21, 40). All cloning was carried out using the *E. coli* strain DH5α grown in lysogeny broth (LB) with the addition of antibiotics at a concentration of 25 μg/mL for kanamycin or chloramphenicol individually and at 10 μg/mL each under double selection. Reagents were acquired from Sigma-Aldrich unless noted otherwise.

Fluorescence Microscopy. The *E. coli* strain DH5α was transformed with pDFS21-GFP, pCsoS1A-GFP, or pCbbL-CFP with or without pHnCB, and single colonies were chosen and grown until late log phase at 30 °C. Log-phase cells were centrifuged, washed in 1× PBS solution, loaded onto 2% agarose pads, and placed in a glass-bottomed dish (MatTek). Cells were imaged using a Nikon TE-2000 microscope equipped with an ORCA-ER CCD camera (Hamamatsu) using standard filter sets for each fluorophore (Chroma).

Electron Microscopy of Whole Cells. *E. coli* strain DH5α was transformed with pHnCB, and single colonies were grown at 37 °C, diluted 1:50 in LB + 50 μM IPTG, and grown until midlog phase. Pellets of cells were fixed for 2 h at room temperature in routine fixative (2.5% glutaraldehyde, 1.25% paraformaldehyde, and 0.03% picric acid in 0.1 M sodium cacodylate buffer; pH 7.4), washed in 0.1 M cacodylate buffer (pH 7.4), and postfixed with 1% osmium tetroxide/1.5% potassium ferrocyanide for 2 h. The pellet was then washed in water three times and incubated in 1% aqueous uranyl acetate for 1 h, followed by two washes in water and subsequent dehydration. The samples were then put in propylene oxide for 1 h and infiltrated overnight. The next day, samples were embedded in Epon (TAAB) and polymerized at 60 °C for 48 h. Finally, ultrathin sections (60 nm) were cut on a Reichert Ultracut-S microtome, stained with lead citrate, and examined in a JEOL 1200EX transmission electron microscope.

In Vivo Carbon Fixation Assay. DH5α cells were transformed with plasmid pHnCB/pPRK, pNS3/PRK, or pNS3/pDFS21 (WT), inoculated into LB, and grown overnight at 37 °C. The cultures were then diluted 1:50 in LB + 20 μM IPTG for 3 h more. Cells in exponential phase were pelleted, washed twice in M9 salts, and resuspended in M9 salts plus 0.2% arabinose, 20 μM IPTG, 20 mM $NaHCO_3$, and 1 μg/mL thiamine, and adjusted to pH 7.0 using HCl. The cells were then incubated at 37 °C with constant shaking, and the optical density at 600 nm was measured continuously in a spectrophotometer (Varian Cary 300 Bio). To prevent evaporation, mineral oil was layered over cultures, and cuvettetes were covered with aluminum foil.

CB Purification. An overnight culture of DH5α transformed with pHnCB was diluted 1:50 and grown at 20 °C overnight in terrific broth or LB. Protein expression was induced with 50 μM IPTG. Cells were lysed with an Emulsiflex-C3 homogenizer (Avestin), and the purification was carried out using a protocol for sucrose gradient centrifugation derived from Cannon and coworkers (31). Fractions from the gradient were assayed using a combination of EM, SDS/PAGE with Coomassie blue staining, Western blot analysis, and RuBisCO activity kinetics to identify fractions enriched in CBs. Typical yields were ~20 mg of purified protein per L of starting culture.

Electron Microscopy of Purified CBs. Purified CBs were adsorbed for 1 min to a carbon-coated grid that had been made hydrophilic by a 30-s exposure to glow discharge. Excess liquid was removed with filter paper (Whatman #1), and the samples were stained with 1.0% uranyl formate for 30 s. After the excess uranyl formate was removed with filter paper, the grids were examined using a JEOL 1200EX, Tecnai G^2 Spirit, or Tecnai 12 transmission electron microscope, and images were recorded with a CCD camera.

Protein Mass Spectrometry. Individual components of the CB-enriched fraction were identified via liquid chromatography–tandem mass spectrometry. The CB fractions were separated using SDS/PAGE and stained with Coomassie brilliant blue to resolve individual species. Bands were cut and sent to the University of California Davis Genome Center Proteomics Core Facility for analysis.

In Vitro Fixation. CO_2 fixation by purified CBs was measured using a 3-phosphoglycerate–dependent enzyme system coupled to NADH oxidation (41). First, 3 μg/mL of purified CBs was added to a reaction buffer containing 100 mM Tris (pH 8.0), 25 mM $NaHCO_3$, 20 mM $MgCl_2$, 10 mM KCl, 3.5 mM ATP, 5 mM creatine phosphate, 2 mM DTT, 0.25 mM NADH, 5 U/mL creatine phosphokinase, 5 U/mL 3-phosphoglycerate kinase, and 5 U/mL NAD-dependent glyceraldehyde 3-phosphate dehydrogenase and allowed to activate for 10 min at 30 °C. After addition of D-ribulose 1,5-bisphosphate, the reaction was mixed and monitored spectrophotometrically at 30 °C by following NADH oxidation in a plate reader (Wallac/Spectromax). Initial enzyme rates were fit to a Michaelis–Menten type model using nonlinear regression in MATLAB (Mathworks) to derive V_{max} and K_m parameters. Kinetic values were normalized using total protein, as assayed by absorption at 280 nm.

ACKNOWLEDGMENTS. We thank Eva Nogales, Gigi Kemalyan, Elizabeth Benecchi, and Maria Ericsson for electron microscopy assistance; Todd Yeates for the carboxysome shell model shown in Fig. 1*A*, and Janet Iwasa for aid with molecular modeling. This work was supported by the Life Sciences

Division of the US Army Research Office (W911NF-09-1-0226), Advanced Research Projects Agency–Energy Grant DE-AR0000079; the Wyss Institute of Biologically Inspired Engineering (P.A.S.); and the Department of Energy Office of Science Early Career Research Program through Office of Basic Energy Sciences Grant DE-SC0006394 (to D.F.S.). D.F.S. was a Department of Energy Physical Biosciences Fellow of the Life Sciences Research Foundation.

1. Alberts B, Johnson A, Lewis J, Raff M, Roberts K (2002) *Molecular Biology of the Cell* (Garland Science, New York), IV.
2. Mitchell P (1961) Coupling of phosphorylation to electron and hydrogen transfer by a chemi-osmotic type of mechanism. *Nature* 191:144–148.
3. Boyle PM, Silver PA (2009) Harnessing nature's toolbox: Regulatory elements for synthetic biology. *J R Soc Interface* 6(Suppl 4):S535–S546.
4. Park SH, Zarrinpar A, Lim WA (2003) Rewiring MAP kinase pathways using alternative scaffold assembly mechanisms. *Science* 299:1061–1064.
5. Dueber JE, et al. (2009) Synthetic protein scaffolds provide modular control over metabolic flux. *Nat Biotechnol* 27:753–759.
6. Kerfeld CA, et al. (2005) Protein structures forming the shell of primitive bacterial organelles. *Science* 309:936–938.
7. Schmid MF, et al. (2006) Structure of *Halothiobacillus neapolitanus* carboxysomes by cryo-electron tomography. *J Mol Biol* 364:526–535.
8. Iancu CV, et al. (2007) The structure of isolated *Synechococcus* strain WH8102 carboxysomes as revealed by electron cryotomography. *J Mol Biol* 372:764–773.
9. Yeates TO, Crowley CS, Tanaka S (2010) Bacterial microcompartment organelles: Protein shell structure and evolution. *Annu Rev Biophys* 39:185–205.
10. Beeby M, Bobik TA, Yeates TO (2009) Exploiting genomic patterns to discover new supramolecular protein assemblies. *Protein Sci* 18:69–79.
11. Shively JM, Ball FL, Kline BW (1973) Electron microscopy of the carboxysomes (polyhedral bodies) of *Thiobacillus neapolitanus*. *J Bacteriol* 116:1405–1411.
12. Heinhorst S, Cannon GC, Shively JM (2006) in *Complex Intracellular Structures in Prokaryotes*, ed Shively JM (Springer, Berlin), pp 141–164.
13. Long BM, Badger MR, Whitney SM, Price GD (2007) Analysis of carboxysomes from *Synechococcus* PCC7942 reveals multiple RuBisCOo complexes with carboxysomal proteins CcmM and CcaA. *J Biol Chem* 282:29323–29335.
14. Kaplan A, Reinhold L (1999) CO_2-concentrating mechanisms in photosynthetic microorganisms. *Annu Rev Plant Physiol Plant Mol Biol* 50:539–570.
15. Price GD, Badger MR, Woodger FJ, Long BM (2008) Advances in understanding the cyanobacterial CO_2-concentrating mechanism (CCM): Functional components, Ci transporters, diversity, genetic regulation and prospects for engineering into plants. *J Exp Bot* 59:1441–1461.
16. Penrod JT, Roth JR (2006) Conserving a volatile metabolite: A role for carboxysome-like organelles in *Salmonella enterica*. *J Bacteriol* 188:2865–2874.
17. Sampson EM, Bobik TA (2008) Microcompartments for B12-dependent 1,2-propanediol degradation provide protection from DNA and cellular damage by a reactive metabolic intermediate. *J Bacteriol* 190:2966–2971.
18. Klein MG, et al. (2009) Identification and structural analysis of a novel carboxysome shell protein with implications for metabolite transport. *J Mol Biol* 392:319–333.
19. Kinney JN, Axen SD, Kerfeld CA (2011) Comparative analysis of carboxysome shell proteins. *Photosynth Res* 109:21–32.
20. Menon BB, Dou Z, Heinhorst S, Shively JM, Cannon GC (2008) *Halothiobacillus neapolitanus* carboxysomes sequester heterologous and chimeric RuBisCO species. *PLoS ONE* 3:e3570.
21. Savage DF, Afonso B, Chen AH, Silver PA (2010) Spatially ordered dynamics of the bacterial carbon fixation machinery. *Science* 327:1258–1261.
22. Parsons JB, et al. (2008) Biochemical and structural insights into bacterial organelle form and biogenesis. *J Biol Chem* 283:14366–14375.
23. Parsons JB, et al. (2010) Synthesis of empty bacterial microcompartments, directed organelle protein incorporation, and evidence of filament-associated organelle movement. *Mol Cell* 38:305–315.
24. Fan C, et al. (2010) Short N-terminal sequences package proteins into bacterial microcompartments. *Proc Natl Acad Sci USA* 107:7509–7514.
25. Cannon GC, et al. (2003) Organization of carboxysome genes in the thiobacilli. *Curr Microbiol* 46:115–119.
26. Price GD, Howitt SM, Harrison K, Badger MR (1993) Analysis of a genomic DNA region from the cyanobacterium *Synechococcus* sp. strain PCC7942 involved in carboxysome assembly and function. *J Bacteriol* 175:2871–2879.
27. Tsai Y, et al. (2007) Structural analysis of CsoS1A and the protein shell of the *Halothiobacillus neapolitanus* carboxysome. *PLoS Biol* 5:e144.
28. Gatenby AA, Ellis RJ (1990) Chaperone function: The assembly of ribulose bisphosphate carboxylase-oxygenase. *Annu Rev Cell Biol* 6:125–149.
29. Parikh MR, Greene DN, Woods KK, Matsumura I (2006) Directed evolution of RuBisCO hypermorphs through genetic selection in engineered *E. coli*. *Protein Eng Des Sel* 19: 113–119.
30. Cannon G, Shively J (1983) Characterization of a homogenous preparation of carboxysomes from *Thiobacillus neapolitanus*. *Arch Microbiol* 134:52–59.
31. So AK-C, et al. (2004) A novel evolutionary lineage of carbonic anhydrase (epsilon class) is a component of the carboxysome shell. *J Bacteriol* 186:623–630.
32. Dou Z, et al. (2008) CO_2 fixation kinetics of *Halothiobacillus neapolitanus* mutant carboxysomes lacking carbonic anhydrase suggest the shell acts as a diffusional barrier for CO_2. *J Biol Chem* 283:10377–10384.
33. Cai F, Heinhorst S, Shively JM, Cannon GC (2008) Transcript analysis of the *Halothiobacillus neapolitanus* cso operon. *Arch Microbiol* 189:141–150.
34. Lal R (2008) Carbon sequestration. *Philos Trans R Soc Lond B Biol Sci* 363:815–830.
35. Tcherkez GGB, Farquhar GD, Andrews TJ (2006) Despite slow catalysis and confused substrate specificity, all ribulose bisphosphate carboxylases may be nearly perfectly optimized. *Proc Natl Acad Sci USA* 103:7246–7251.
36. Rabaey K, Rozendal RA (2010) Microbial electrosynthesis: Revisiting the electrical route for microbial production. *Nat Rev Microbiol* 8:706–716.
37. Douglas T, Young M (2006) Viruses: Making friends with old foes. *Science* 312: 873–875.
38. Nam KT, et al. (2006) Virus-enabled synthesis and assembly of nanowires for lithium ion battery electrodes. *Science* 312:885–888.
39. Flynn C (2003) Viruses as vehicles for growth, organization and assembly of materials. *Acta Mater* 51:5867–5880.
40. Niederholtmeyer H, Wolfstädter BT, Savage DF, Silver PA, Way JC (2010) Engineering cyanobacteria to synthesize and export hydrophilic products. *Appl Environ Microbiol* 76:3462–3466.
41. Lilley RM, Walker DA (1974) An improved spectrophotometric assay for ribulosebisphosphate carboxylase. *Biochim Biophys Acta* 358:226–229.